Differentiable simulation to develop molecular dynamics force fields for disordered proteins

Joe G Greener
Medical Research Council Laboratory of Molecular Biology
Cambridge, UK
jgreener@mrc-lmb.cam.ac.uk

Abstract

Implicit solvent force fields are computationally efficient but can be unsuitable for running molecular dynamics on disordered proteins. Here I improve the a99SB-*disp* force field and the GBNeck2 implicit solvent model to better describe disordered proteins. Differentiable molecular simulations with 5 ns trajectories are used to jointly optimise 108 parameters to better match explicit solvent trajectories. Simulations with the improved force field better reproduce the radius of gyration and secondary structure content seen in experiments, whilst showing slightly degraded performance on folded proteins and protein complexes. The force field, called GB99dms, reproduces the results of a small molecule binding study and improves agreement to experiment for the aggregation of amyloid peptides. GB99dms, which can be used in OpenMM and is available at `https://github.com/greener-group/GB99dms`, is useful for simulating a range of protein systems. This work is the first to show that gradients can be obtained directly from nanosecond-length differentiable simulations of biomolecules and highlights the effectiveness of this approach to training whole force fields to match desired properties.

Introduction

Molecular dynamics (MD) simulations have helped us to understand how molecules move [1, 2], and will only become more important as computers get faster and innovative machine learning approaches are developed [3, 4]. There are two main issues with MD: the force fields used to describe atomic interactions lack accuracy, and sampling beyond the microsecond scale is computationally prohibitive. When simulating a biomolecular system it is usually the solute that is of interest, so implicit solvent models can be used to replace solvent molecules with a continuous medium [5, 6]. This speeds up simulations by reducing the number of atoms and by giving faster exploration of conformational space due to the lack of friction with solvent [7]. Despite the lack of interactions between the solute and individual solvent molecules being a fundamental limitation of implicit solvent models, they are regularly used across a range of biomolecular simulations [8] and have been the target of machine learning approaches [9]. Small proteins can be folded in GPU-days with implicit solvent models and enhanced sampling [10], whereas with explicit solvent it would have taken considerably longer.

Major inaccuracies of implicit solvent models include the tendency to overcompact disordered proteins into rigid, often α-helical structures, the tendency to cause any pair of proteins to bind strongly, and the poor secondary structure match to experiments for peptides [11, 12, 13, 14]. There has been considerable recent effort to alleviate related, and less severe, problems for explicit solvent force fields [15, 16, 17], resulting in a better match to experimental data for both folded and disordered proteins [18, 19, 20, 21]. This forms part of a wider attempt to use data to improve force fields [22, 23, 24, 25]. However there has been less attention on improving implicit solvent models in this area [26], with notable exceptions being the ABSINTH model [27] and coarse-grained approaches that

combine multiple atoms into one site [28, 29]. This is a missed opportunity: despite their fundamental limitations, implicit solvent models need not perform as poorly as they do on disordered systems. In fact they are especially well-suited to studying these systems, as they are not slowed by the large solvent boxes required for explicit solvent simulations and can be used to probe slow events such as protein aggregation [30, 31] with the increased conformational sampling resulting from low viscosity [7]. Whereas explicit solvent force fields have been improved in tandem with associated water models [32, 33, 34, 35], this is rarely the case for implicit solvent models [11, 36], suggesting that adjusting both at the same time could lead to improvements.

In this study I modify the parameters of an existing force field and implicit solvent model to better describe disordered proteins and protein aggregation, whilst retaining acceptable performance on folded proteins. The technique of differentiable molecular simulation (DMS) is used to modify many force field parameters at the same time. This emerging technique allows structural and dynamic properties to be targeted to parameterise whole force fields using automatic differentiation (AD) [37]. This is part of the paradigm of differentiable programming [38] in which AD, more commonly associated with training neural networks, is used to obtain gradients from arbitrary algorithms. DMS has previously been used to train a coarse-grained force field for proteins from scratch [39], to learn pairwise potentials [40, 41], for enhanced sampling [42], to predict protein structure [43] and to explore statistical physics models [44]. Dedicated software packages such as Jax MD [45], TorchMD [46] and DMFF [47] have been developed specifically for differentiable simulations. The Molly.jl software developed as part of this work provides a flexible and fast option for DMS and for MD more broadly. The combined force field and implicit solvent model presented here, called GB99dms, is available to the community for simulating a range of protein systems and is easy to run from OpenMM. Here it is shown for the first time that DMS can be used to train force fields over nanosecond-length simulations.

Results

There are a number of recent software packages designed for DMS [45, 46, 47]. However all were either lacking features for simulating proteins or did not have the performance required to do AD on simulations of millions of steps. Hence the capabilities of the Julia [48, 49] package Molly.jl were expanded to carry out training simulations for this work. This package is a pure Julia implementation of MD compatible with biomolecules and DMS which implements various integrators and allows easy definition of custom interactions. Code is run on the GPU using kernels written in Julia with CUDA.jl [50, 51]. Gradients are computed using Zygote.jl [52] and Enzyme.jl [53, 54]. Together these allow gradients to be computed through arbitrary code on the GPU, including complicated algorithms such as the force calculation of GBNeck2. Reverse-mode AD is used as it has constant compute time with respect to the number of parameters. However, broadcasted functions do use an efficient combined forward and reverse approach [55].

I choose to start from the a99SB-*disp* force field [20] since it has been developed for both folded and disordered proteins, and the GBNeck2 implicit solvent model [56] since it shows good performance on folded proteins [10]. The a99SB-*disp* modified backbone O-H interaction term is not used, as it was later found to not impact the ability to fit quantum mechanical data [21]. Since some atom types in the force field appear rarely in the training data, parameters are modified for 16 common atom types: CA, CT, C, C8, C9, N, N3, O, O2, OH, H, H1, HA, HC, HO and HP. This gives 108 parameters to change: partial charge scaling, Lennard-Jones (LJ) σ and LJ ε for the 16 atom types (46 non-zero parameters); torsion k values for 13 common proper torsions (33); LJ and Coulomb 1-4 interaction scalings (2); GBNeck2 atom radii (6); GBNeck2 atom parameters (12); GBNeck2 screening parameters (4); and the GBNeck2 parameters neck cutoff, neck scale, offset, probe radius and surface area factor (5). To maintain the overall charge of residues the partial charges are not changed directly, instead a charge scaling is learned - see the methods. Torsion phases, which in a99SB-*disp* are all symmetrical around 0 degrees apart from backbone φ and ψ, are not modified as this has questionable physical

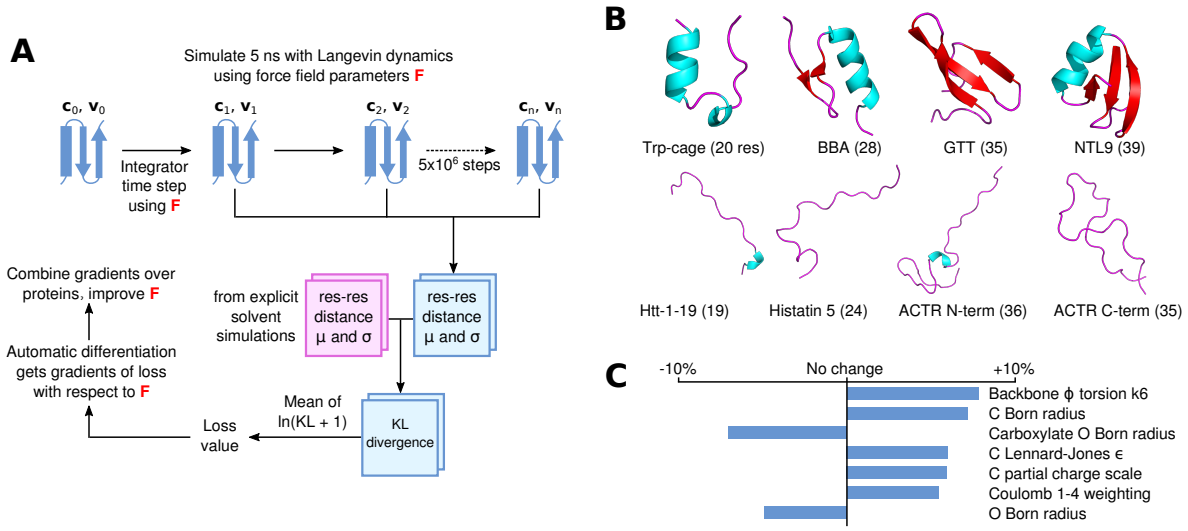

Figure 1 Differentiable molecular simulation to improve an implicit solvent force field. (A) For each protein a simulation is run with Langevin dynamics and the mean (μ) and standard deviation (σ) of the Cα residue-residue distances are calculated. These are compared using the KL divergence to corresponding values from reference explicit solvent simulations to obtain a loss value. AD is then used to obtain gradients of the loss with respect to the force field parameters, which can be used to improve the force field. (B) The 8 proteins used for training, consisting of 4 folded proteins (top) and 4 disordered proteins (bottom). (C) The 7 parameters that change by at least 4.5% in absolute value from the starting values in a99SB-*disp*+GBNeck2.

validity.

8 small proteins ranging in size from 19 to 39 residues, 4 folded and 4 disordered, are used for training. These are shown in Figure 1B. The folded proteins are Trp-cage (PDB ID 2JOF), BBA (1FME), GTT (2F21) and NTL9 (2HBA) and contain both α-helices and β-sheets. The disordered proteins are Htt-1-19, a slightly helical intrinsically disordered protein (IDP) derived from huntingtin's N-terminus; histatin-5; and the N-terminal and C-terminal halves of ACTR, split up to avoid excessive computational demands during training. At each epoch of training, each protein is simulated using a Langevin integrator with the current force field parameters for 5 ns (5 million steps). Residue-residue distances are periodically recorded and used at the end of the simulation to calculate the mean and standard deviation for each residue-residue distance over the simulation. Since explicit solvent simulations with the a99SB-*disp* force field and its corresponding water model seem to accurately describe the properties of both folded and disordered proteins [20], I train to match the residue-residue distances in 2 μs simulations of the training proteins with this force field. Previous approaches to developing implicit solvent force fields have also matched to explicit solvent data [57].

The Kullback-Leibler (KL) divergence is calculated in both directions between the training and reference simulations, and averaged over residues. This gives a loss value; since the simulation is implemented in AD-compatible software, the gradients of the loss with respect to the force field parameters can be calculated. These are combined across the training proteins and used to change the force field parameters, before the next epoch is started. Simulations of the folded proteins start from the PDB coordinates and a single repeat is run. For the disordered proteins two repeats are run, starting from different snapshots of the reference explicit solvent simulations. Each 5 ns simulation takes 15-24 hours on a GeForce RTX 2080 Ti GPU depending on the size of the protein. The parameters after 5 epochs

of training are used, meaning training takes 5 days on 12 GPUs. This overall training process is shown in Figure 1A.

The parameters of the trained force field, named GB99dms, are similar to the starting parameters, with only 19 out of 108 parameters changing by more than 3% in absolute value. Staying close to the starting values was a deliberate attempt to find a point in the high-dimensional parameter space that works across a variety of protein systems but remains similar to the well-studied parameters available currently [58]. The direction of parameter changes are generally consistent across epochs of training, as shown in Figure S1. The parameters that change the most are shown in Figure 1C and all parameters are listed in Table S1. The Born radius parameters for carbonyl O and backbone amide H decrease, indicating less screening from solvent, though the Born radius parameters for C and H increase. The LJ σ parameters for N and C increase, indicating a larger interaction distance for these atoms. The LJ ε parameters increase for N and C but decrease for HC and CT, indicating a shift in strength of LJ interactions between atom types. Small changes are made to torsion parameters; as expected due to the required changes in secondary structure preferences, backbone φ and ψ change the most. Partial charges do not change much, except C which becomes more positive (0.597 to 0.625 for backbone carbonyl C in alanine). The Coulomb and LJ 1-4 interaction weightings for atoms separated by 3 bonds both increase, indicating less shielding from non-bonded forces for nearby atoms. Whilst the bonded/non-bonded parameters and implicit solvent parameters of this force field could be used separately in future, this was not tested and it is recommended that they are used together as they were trained.

GB99dms was compared to existing force fields on a set of proteins not homologous to those used for training. I compare to the combination of Amber ff14SBonlysc [10, 60] and GBNeck2 [56] used successfully to fold proteins [10] and to the combination of a99SB-*disp* [20] and GBNeck2 used at the start of training in this work. First, performance is assessed on 8 IDPs ranging in size from 40 to 140 residues. This is the set used in Robustelli et al. 2018 [20], excluding ACTR which is used here for training. For each protein 3 simulations of 2 µs were run for each force field, with an initial burn-in period of 0.5 µs starting from an extended conformation being discarded. All validation simulations were run with a Langevin collision frequency γ of 1 ps^{-1} to increase conformational sampling. As shown in Figure 2 the radius of gyration (R_g) using GB99dms matches experimental data [20] and observed scaling laws [59] considerably better than the existing force fields across a range of protein sizes. Figure 2C and Figure S2 indicate that this is partly due to existing force fields giving structures that are too α-helical and inflexible, and Figure S2 shows that the experimental R_g may be sampled with GB99dms even when the mean simulation R_g is different. There is still some discrepancy between GB99dms and experiment, for example in the location of α-helices in Ntail and PaaA2, in line with the variety of secondary structure propensities shown previously by explicit solvent force fields for these IDPs [20].

Having established improved performance on IDPs, it is important to test whether performance has degraded for folded proteins. 3 simulations of 2 µs for each force field were run on the 4 folded proteins in Robustelli et al. 2018 [20], ranging in size from 56 to 129 residues: GB3 (PDB ID 1P7E), ubiquitin (1D3Z), hen egg white lysozyme (HEWL, 6LYZ) and bovine pancreatic trypsin inhibitor (BPTI, 5PTI). Figure 3A shows the root-mean-square deviation (RMSD) to the native structure across the trajectory for each simulation. GB3 and ubiquitin show similar stability over the simulations with all 3 force fields. HEWL and BPTI show less stability with GB99dms. For HEWL 3 of the α-helices and the β-sheet lose their secondary structure, though the overall tertiary structure remains the same. For BPTI the β-sheet remains intact but the α-helices lose their secondary structure and the loops show significant flexibility. The difficulty of balancing secondary structure preferences in implicit solvent force fields has been established previously [12].

Performance is also assessed on 4 medium-sized protein dimers from Piana et al. 2020 [21] ranging in size from 197 to 235 total residues: barnase/barstar (PDB ID 1X1X), colE7/Im7 (7CEI), SGPB/OMTKY3 (3SGB) and CD2/CD58 (1QA9). There has been less work on developing and assessing implicit solvent

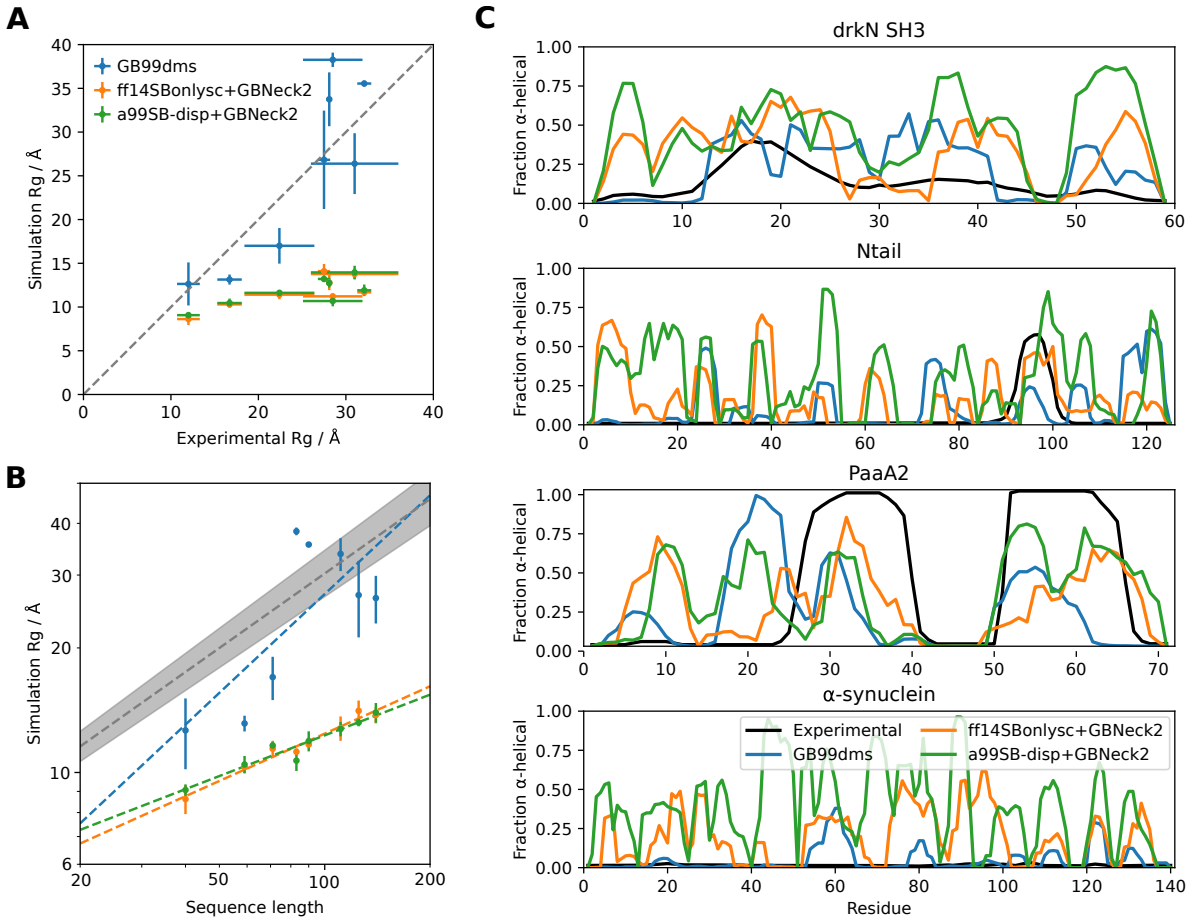

Figure 2 The behaviour of IDPs with implicit solvent force fields. The 8 IDPs are Aβ40 (40 residues), drkN SH3 (59), PaaA2 (71), Ash1 (83), Sic1 (90), p15PAF (111), NTail (125) and α-synuclein (140). Experimental values for R_g and α-helical content are taken from Robustelli et al. 2018 [20]. (A) Comparison of simulation and experimental R_g. Each point is the mean R_g over 3 simulations of 2 µs, with an initial burn-in period of 0.5 µs starting from an extended conformation being discarded for each simulation. The error bars in the x direction represent uncertainty in the experimental value and error bars in the y direction represent 95% confidence intervals of the mean calculated from the standard error of the mean across the 3 simulations. The dotted line represents equal experimental and simulation values. (B) Comparison of simulation R_g to sequence length for the same data. The dotted grey line represents the experimentally observed power law relationship $R_G = R_0 N^v$ with $v = 0.598 \pm 0.028$ and $R_0 = 1.927$ Å [59]. The shaded grey area represents the 95% confidence interval of v. The best fit v values from the simulation data for GB99dms, ff14SBonlysc+GBNeck2 and a99SB-*disp*+GBNeck2 are 0.793, 0.380 and 0.327 respectively. (C) α-helical content of IDPs over the same simulations.

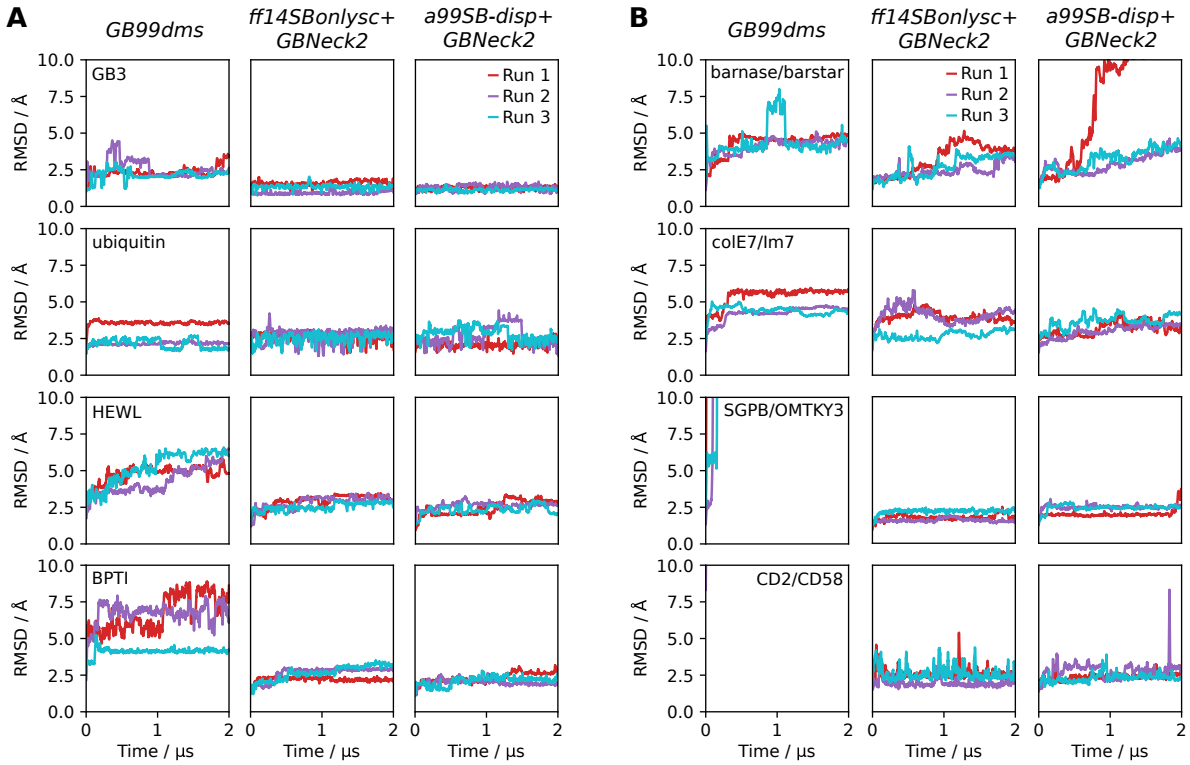

Figure 3 The behaviour of folded proteins and protein complexes with implicit solvent force fields. RMSD to the PDB starting structure is shown over 3 x 2 µs simulations. Snapshots are recorded every 0.5 ns and the mean RMSD of a window extending 10 snapshots either side of the given snapshot is shown. (A) Behaviour of 4 folded proteins. (B) Behaviour of 4 protein dimers. Dissociation occurs within 1 ns for CD2/CD58.

force fields for protein complexes, but here it is found that the 4 dimers are generally stable under the two existing force fields. Figure 3B indicates that with GB99dms barnase/barstar and colE7/Im7 seem stable, though SGPB/OMTKY3 and CD2/CD58 dissociate quickly. The dissociating complexes have less favourable experimental association free energy than those that remain bound [21]. With a collision frequency γ of 91 ps^{-1} more representative of bulk solvent, SGPB/OMTKY3 remains bound at 5 Å after 2 µs RMSD but CD2/CD58 still dissociates. The difficulty of improving performance on IDPs whilst not allowing protein complexes to dissociate has also been encountered with explicit solvent force fields [20, 21]. Overall GB99dms has slightly degraded performance on folded proteins, though could still be useful for studying systems containing a mix of folded and disordered proteins.

MD simulations can be used to study the interactions of small molecules with IDPs, assisting in the difficult process of finding drugs to target the many IDPs implicated in disease. For example, a recent study [61] used a99SB-*disp* to carry out 1.5 ms of explicit solvent simulation of α-synuclein with the small molecule fasudil. α-synuclein is associated with Parkinson's disease and fasudil has been shown to delay α-synuclein aggregation [62]. The contact probability over the simulation of each residue with fasudil was shown to agree with NMR data, allowing an interpretation to be made of how the drug affects the protein. I carried out similar simulations, using the faster sampling of implicit solvent to compare 5 simulations of 2 µs with the NMR data and significantly longer explicit solvent simulations from Robustelli et al. 2022 [61]. Figure 4A shows that GB99dms reproduces a similar profile to the NMR data. There is elevated contact probability in the residue 121-140 C-terminal region, peaks around residues 5-9/39-44/59-72/121-127/136-138, and Y136 has the highest contact probability. In contrast, ff14SBonlysc shows blocks of interacting residues consistent with fasudil interacting with the surface of a compact, inflexible structure and a99SB-*disp* shows consistent and lower interaction throughout the protein. The Pearson correlation coefficients between the contact probabilities and the NMR chemical shift perturbation data are 0.44, 0.10 and 0.07 for GB99dms, ff14SBonlysc and a99SB-*disp* respectively, compared to 0.67 for the explicit solvent simulations [61]. This indicates that GB99dms could be useful for assessing small molecule binding to IDPs during drug discovery. Though it is unusual to use periodic boundary conditions with implicit solvent - one advantage of implicit solvent is not having to deal with boundaries - it is possible since the solvent behaviour is unrelated to the boundary.

Finally, I investigate the behaviour of aggregating peptides with GB99dms. It has previously been shown that the oligomerisation behaviour under simulation of the 7-residue aggregating core of amyloid beta (Aβ), $A\beta_{16\text{-}22}$, depends on the force field and does not always reproduce the effect of mutations [63, 64]. Here I study the oligomerisation of 6 capped $A\beta_{16\text{-}22}$ peptides in a periodic box. I simulate 3 x 2 µs with each force field for 3 peptide sequences: the wild-type KLVFFAE, the F19L mutant which aggregates faster than wild-type, and the F19V/F20V double mutant which does not aggregate [64]. All force fields show oligomerisation of all 6 peptides within 2 µs. As shown in Figure 4B, GB99dms reproduces best the observed behaviour of the sequences: on average F19L forms oligomers fastest and F19V/F20V slowest. The wild-type forms oligomers faster than F19L for ff14SBonlysc and F19V/F20V forms oligomers at a similar speed to wild-type for ff14SBonlysc and a99SB-*disp*. The final oligomers adopt extended monomer conformations for GB99dms reminiscent of Aβ fibrils, whereas for ff14SBonlysc and particularly a99SB-*disp* the conformations are more α-helical. These results show that GB99dms could be used to study amyloid aggregation at scale. One advantage of implicit solvent is that the periodic box size, and hence the effective concentration of Aβ, can be changed without adding more atoms. Currently, high concentration is a limitation of many MD studies of aggregation [30].

Discussion

Recently much effort has gone into developing machine learning interatomic potentials (MLIPs), which show quantum mechanical-level accuracy at faster speeds. Whilst these are promising, I believe that the

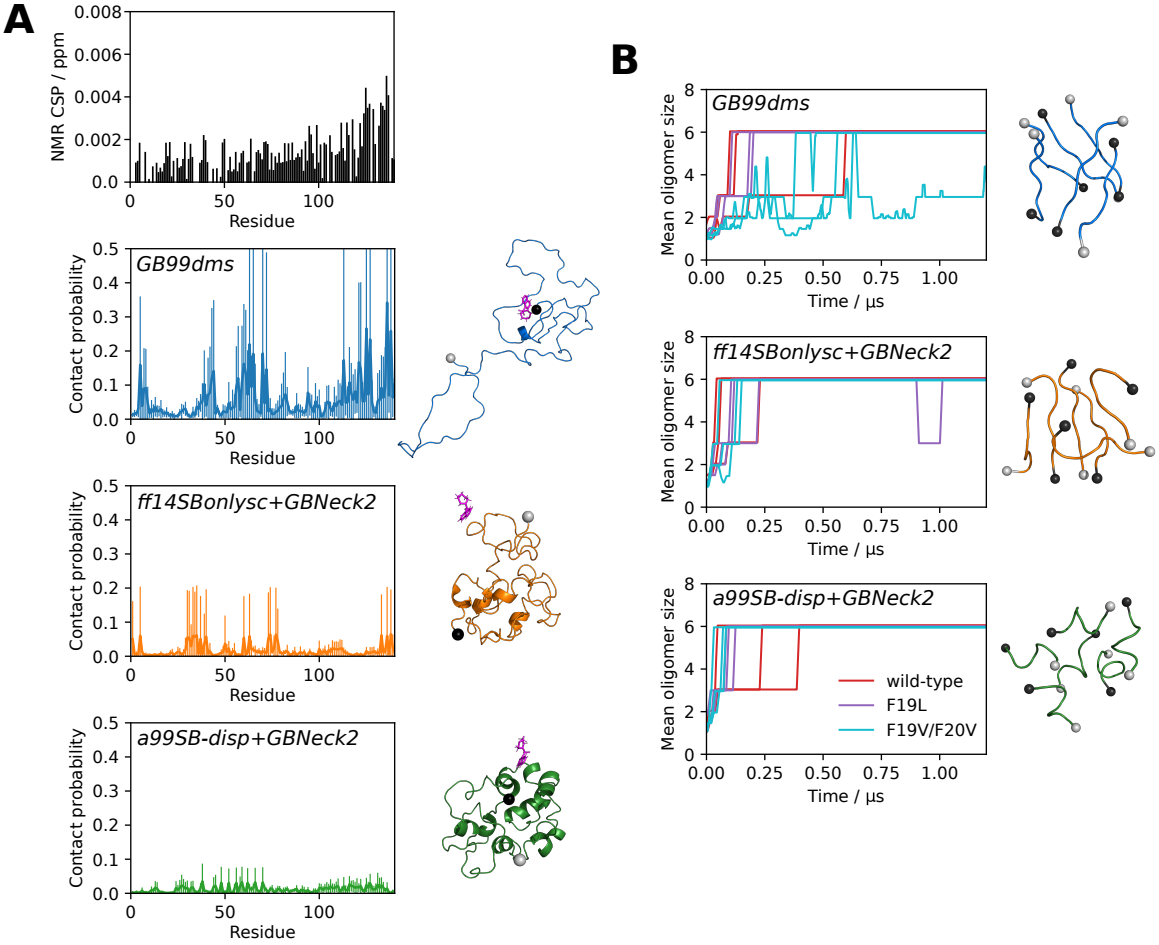

Figure 4 Ligand binding and amyloid aggregation with implicit solvent force fields. Grey and black spheres on structures represent the N- and C-termini respectively. (A) The interaction of α-synuclein and the small molecule fasudil. The NMR chemical shift perturbation (CSP) data from Robustelli et al. 2022 [61] is shown. The fraction of the time each residue is in contact with fasudil over 5 x 2 µs simulations is shown for each force field, along with a snapshot where fasudil is in contact with α-synuclein. The error bars for each residue represent 95% confidence intervals of the mean calculated from the standard error of the mean across the 5 simulations. (B) Oligomerisation of 6 x $A\beta_{16\text{-}22}$. Three capped peptides are studied: KLVFFAE (wild-type), F19L (faster aggregation) and F19V/F20V (no aggregation). The oligomer size over 3 x 2 µs simulations is shown for each sequence and force field. Repeats are shown separately, with the plots truncated at 1.2 µs as there is little change beyond this time. Snapshots are recorded every 0.5 ns and the mean oligomer size of a window extending 10 snapshots either side of the given snapshot is shown. The final oligomer from the first wild-type repeat is also shown.

techniques of machine learning can also be used to improve molecular mechanics force fields by effective optimisation of their large parameter spaces [65, 58]. This retains the advantages of interpretability, robustness and speed given by molecular mechanics force fields over MLIPs. The smooth nature of these force fields - at least compared to the hard potentials used in domains such as robotics simulations - makes them well-suited to differentiable simulation. An advantage of DMS over force-matching approaches is that targeting global structural properties alleviates issues when simulations reach states not seen in their training data, a problem that can lead to a lack of stability for MLIPs as errors accumulate during simulation [66]. Another advantage is that existing experimental data can be used, rather than the large amount of quantum mechanical data required to train accurate and transferable MLIPs.

The simulations of 5 million steps carried out in this work are the longest differentiable molecular simulations to date and indicate that even longer simulations are possible. The next step is to train an all-atom explicit solvent force field using DMS to match experimental data such as NMR constraints. This will require improvements in computational speed, as well as differentiable implementations of algorithms such as bond constraints and Ewald summation that could run into the limitations of AD [67]. The flexibility of the approach allows it to be combined with other recent advances such as continuous atom typing with graph neural networks [68] and exploration of different functional forms for non-bonded interactions [69]. One promising approach, Time Machine (`https://github.com/proteneer/timemachine`), aims to use DMS for drug discovery.

A question surrounding DMS is whether accurate gradients can be obtained through long MD simulations. Gradients could explode or vanish, and there are also concerns about error propagation over long, chaotic simulations [70, 42, 43, 71]. Here, I find that the Langevin integrator is effective at propagating gradients using reverse-mode AD. By contrast, simulations in the NVE ensemble were not found to produce stable gradients. The stochastic noise applied to every atom at every step in Langevin dynamics likely provides a regularisation effect that helps prevent gradient explosion but does not lead to vanishing gradients [72]. This stochasticity, along with the random starting velocities, means that the gradients are a sample over a distribution. When repeating runs, typically over 80% of the parameter gradients have the same sign and the Pearson correlation coefficient of parameter gradients is over 0.8. Good correlation is also found when comparing simulations run with a 1 fs and a 0.5 fs time step, and when comparing simulations run with single or double precision floating point numbers throughout. This justifies the decision to use a 1 fs time step and single precision for computational efficiency. Adjoint sensitivity methods provide another way to obtain gradients through simulations [73, 74, 41], but are often unstable and have had less development than reverse-mode AD. Here I find that the "simple" approach of using AD on the integrator works well.

Another question is whether the computational overhead of calculating the gradients via AD makes it worthwhile compared to using a black box approach such as finite differencing. Our Julia code is currently 100-1000x slower on the GPU when gradients are required than heavily optimised non-differentiable codes such as OpenMM [75] and Gromacs [76]. However the gradients for all parameters are calculated to numerical accuracy in one go, whereas a number of runs would be required per gradient when using finite differencing. It seems that the current case of optimising 108 parameters is around the crossover point, and optimising any fewer parameters would have been easier with finite differencing. As DMS code becomes faster and more parameters are included for training, for example more atom types or torsion CMAP potentials, the advantage of DMS will become clearer. One direction of future work is to improve the performance of the Julia code significantly using more advanced GPU kernels [50] and further use of the Enzyme AD framework [53, 54]. It remains an open question how close in performance a differentiable implementation can get to a non-differentiable one. Molly.jl will be useful for exploring these questions, and for training the next generation of force fields that are transferable, reproducible and fast.

Methods

The a99SB-*disp* force field was manually converted from Desmond/Gromacs files to the OpenMM XML force field format with the modified backbone O-H interaction term omitted. Training simulations were carried out with Molly.jl, which is available along with documentation at `https://github.com/JuliaMolSim/Molly.jl` and will be described fully in a future publication. Training simulations were carried out for 5 ns using a Langevin integrator with a γ of 0.1 ps^{-1}, a 1 fs time step, a temperature of 300 K and no distance cutoff for non-bonded interactions. A Debye-Hückel screening parameter $\varkappa$ of 0.7 nm^{-1} was used [77]. This is roughly equivalent at 300 K to a salt concentration of 100 mM, which is similar to that used when simulating biomolecules under physiological conditions. Energy minimisation but not equilibration was carried out. The low time step was used because bonds were not constrained. The low γ was used to maximise conformational exploration during the 5 ns simulations. Single precision was used for all floating point values, which gave a significant speedup without a noticeable change in gradient accuracy. Reverse-mode AD has a memory cost proportional to the number of steps in the simulation, which quickly becomes prohibitive. This is alleviated with gradient checkpointing. The simulation is run and the state and random seed are saved every 100 steps; during the reverse pass to get gradients, each block of 100 steps is re-run using the corresponding random seed. Gradient clipping was necessary to prevent gradient explosion. Every 100 steps the norm of the gradients on the coordinates and velocities are calculated, and the gradients are rescaled to have a norm of 0.1 if either norm is greater than 0.1.

Every 5 ps (5000 steps), the Cα residue-residue distances X and square distances X^2 are recorded. At the end of the simulation, the mean $\mu_s = E[X]$ and standard deviation $\sigma_s = \sqrt{E[X^2] - (E[X])^2}$ of the Cα residue-residue distances are calculated. For each residue pair, the KL divergence D_{PQ} to the reference explicit solvent distances (see below) is calculated as

$$D_{PQ} = \log\left(\frac{\sigma_r}{\sigma_s}\right) + \frac{\sigma_s^2 + (\mu_s - \mu_r)^2}{2\sigma_r^2} - \frac{1}{2}$$

where μ_r and σ_r are the mean and standard deviation of the reference residue pair distances respectively. The KL divergence in the other direction D_{QP} is also calculated. The loss for each residue pair L_{ij} is then calculated as

$$L_{ij} = \ln(D_{PQ} + 1) + \ln(D_{QP} + 1)$$

In order to reduce the impact of large losses from residue pairs close in sequence with sharp residue-residue distance distributions, the loss of close residue pairs is downweighted. This meant multiplying L_{ij} by a weighting factor which is 0 for residue separation $|i - j| = 0$, 1 for $|i - j| \geq 10$ and linearly spaced between. The overall loss is then calculated as the mean of these weighted values over all residue pairs. AD is used to calculate the gradient of this loss with respect to each of the 108 parameters.

At each epoch of training, gradients are combined from simulations of the 8 training proteins to update the force field. For the IDPs, gradients are averaged over the two repeats. For each protein the gradients are then divided by the median of the absolute values of the gradients, meaning that all proteins contribute similarly to the parameter updates each epoch even if the gradient sizes differ. The gradients for LJ σ parameters and hydrogen parameters were found to be large compared to other parameters and large changes in these parameters can quickly lead to instabilities, so the gradients were weighted by a factor of 0.02. The absolute change for each parameter per protein per epoch was limited to 0.5% and the combined absolute change for each parameter per epoch was limited to 3%. Parameters were updated by gradient descent using a learning rate of 4×10^{-4}. Training was repeated 3 times and the run with the best performance on the training set was used.

Instead of modifying a partial charge value for each atom type directly, which is complicated by the need to maintain overall charge and by the different partial charges of the same atom type in different residue types, a charge scaling value is learned instead. This starts at one for each atom type. After it is updated during training, partial charges are computed for each atom in a residue type by scaling

the starting partial charge by the scaling value and subtracting an offset. This offset is the difference between the starting and scaled overall charge of the residue multiplied by the fraction of the sum of absolute charges present on the atom after scaling. In effect the change in a partial charge of an atom is compensated for by the partial charges of the other atoms in the residue. This allows one charge scaling value to be learned per atom type but the overall charge of each residue type to remain constant during training.

Explicit solvent trajectories used to get reference residue-residue distances for training were generated with Gromacs v2021.4 [76]. For folded proteins the starting structure was the PDB structure. For disordered proteins the starting structure was the collapsed conformation at the end of a short implicit solvent simulation with a99SB-*disp*+GBNeck2 starting from an extended conformation. The box size was 6 nm for Htt-1-19 and histatin-5 and 7 nm for the two halves of ACTR. These simulations use a Verlet leap frog integrator, a 2 fs time step, constrained bonds to hydrogen, a temperature of 300 K, a 1.2 nm cutoff for non-bonded interactions and particle mesh Ewald treatment of long range electrostatics. Energy minimisation, a 100 ps NVT equilibration and a 100 ps NPT equilibration with position restraints to protein heavy atoms preceded a 2 µs production run in the NPT ensemble, with snapshots saved every 50 ps. Mean and standard deviation residue-residue distances were calculated for the last 1 µs of simulation.

Once the force field parameters have been improved via training, simulations can be run with any MD package that supports the GBNeck2 implicit solvent model. Here OpenMM v8.0.0 [75] is used to run the validation simulations as it has high GPU performance and modifying force field parameters is easy. All validation simulations used a Langevin integrator with a γ of 1 ps^{-1}, a 4 fs time step, constrained bonds to hydrogen, hydrogen mass repartitioning with a factor of 2, a temperature of 300 K, a 2 nm cutoff for non-bonded interactions and a $\varkappa$ value of 0.7 nm^{-1}. Energy minimisation and a 500 ps temperature equilibration with position restraints to heavy atoms preceded production runs, with snapshots saved every 500 ps. Dimers were simulated with no periodic boundaries. Trajectory data was analysed with MDAnalysis [78] and secondary structure was calculated with MDTraj [79]. BioStructures.jl was also used for processing protein structural data [80].

For the simulations of α-synuclein with fasudil, GAFF [81] was used to obtain the force field parameters for fasudil. For each force field, 5 repeats were run starting from different snapshots from α-synuclein monomer simulations. Packmol [82] was used to pack one molecule each of α-synuclein and fasudil in a periodic cubic box with 25 nm sides. A contact is assigned to MD frames where the minimum distance between any fasudil atom and any heavy atom of a residue side chain (CA for glycine) is less than 6 Å [61]. For the $A\beta_{16\text{-}22}$ simulations a periodic cubic box with 21.5 nm sides and 6 peptides were used, corresponding to a concentration of 1 mM. The N- and C-termini of the peptides were capped with acetyl (ACE) and *N*-methlyamide (NME) groups respectively to match experimental conditions. Starting conformations for each peptide were taken from snapshots of a short monomer simulation. For each force field and sequence, 3 repeats were run starting from different packings of 6 peptides generated with Packmol. Oligomer size was determined based on groups of contacting peptides, where any pair of atoms being within 4 Å indicates a contact between peptides [64].

Data and code availability

The trained GB99dms force field in OpenMM XML format, training scripts, simulation scripts and data are available at under a permissive license at `https://github.com/greener-group/GB99dms`. The Molly.jl software used for training is available at `https://github.com/JuliaMolSim/Molly.jl`. Simulation trajectories are available at `https://zenodo.org/record/8298226`.

Acknowledgements

I thank the Sjors Scheres group and Conny Yu for useful discussions; all contributors to Molly.jl; William Moses and Valentin Churavy for support with Enzyme.jl; and Jake Grimmett, Toby Darling

and Ivan Clayson for help with high-performance computing. This work was supported by the Medical Research Council.

References

[1] S A Hollingsworth and R O Dror. Molecular Dynamics Simulation for All. *Neuron*, 99(6):1129–1143, 2018.

[2] K Lindorff-Larsen, S Piana, R O Dror, and D E Shaw. How fast-folding proteins fold. *Science*, 334(6055):517–520, 2011.

[3] O T Unke, M Stöhr, S Ganscha, T Unterthiner, H Maennel, S Kashubin, D Ahlin, M Gastegger, L M Sandonas, A Tkatchenko, and K-R Müller. Accurate Machine Learned Quantum-Mechanical Force Fields for Biomolecular Simulations. *arXiv*, 2205.08306, 2022.

[4] J M Jumper, N F Faruk, K F Freed, and T R Sosnick. Trajectory-based training enables protein simulations with accurate folding and Boltzmann ensembles in cpu-hours. *PLoS Comput Biol*, 14(12):e1006578, 2018.

[5] A V Onufriev and D A Case. Generalized Born Implicit Solvent Models for Biomolecules. *Annu Rev Biophys*, 48: 275–296, 2019.

[6] J Kleinjung and F Fraternali. Design and application of implicit solvent models in biomolecular simulations. *Curr Opin Struct Biol*, 25(100):126–134, 2014.

[7] R Anandakrishnan, A Drozdetski, R C Walker, and A V Onufriev. Speed of conformational change: comparing explicit and implicit solvent molecular dynamics simulations. *Biophys J*, 108(5):1153–1164, 2015.

[8] S Izadi, R Anandakrishnan, and A V Onufriev. Implicit Solvent Model for Million-Atom Atomistic Simulations: Insights into the Organization of 30-nm Chromatin Fiber. *J Chem Theory Comput*, 12(12):5946–5959, 2016.

[9] Y Chen, A Krämer, N E Charron, B E Husic, C Clementi, and F Noé. Machine learning implicit solvation for molecular dynamics. *J Chem Phys*, 155(8):084101, 2021.

[10] H Nguyen, J Maier, H Huang, V Perrone, and C Simmerling. Folding simulations for proteins with diverse topologies are accessible in days with a physics-based force field and implicit solvent. *J Am Chem Soc*, 136(40):13959–13962, 2014.

[11] Q Shao and W Zhu. Assessing AMBER force fields for protein folding in an implicit solvent. *Phys Chem Chem Phys*, 20(10):7206–7216, 2018.

[12] E J M Lang, E G Baker, D N Woolfson, and A J Mulholland. Generalized Born Implicit Solvent Models Do Not Reproduce Secondary Structures of De Novo Designed Glu/Lys Peptides. *J Chem Theory Comput*, 18(7): 4070–4076, 2022.

[13] M S Shell, R Ritterson, and K A Dill. A test on peptide stability of AMBER force fields with implicit solvation. *J Phys Chem B*, 112(22):6878–6886, 2008.

[14] R B Best. Computational and theoretical advances in studies of intrinsically disordered proteins. *Curr Opin Struct Biol*, 42:147–154, 2017.

[15] S Piana, J L Klepeis, and D E Shaw. Assessing the accuracy of physical models used in protein-folding simulations: quantitative evidence from long molecular dynamics simulations. *Curr Opin Struct Biol*, 24:98–105, 2014.

[16] S Rauscher, V Gapsys, M J Gajda, M Zweckstetter, B L de Groot, and H Grubmüller. Structural Ensembles of Intrinsically Disordered Proteins Depend Strongly on Force Field: A Comparison to Experiment. *J Chem Theory Comput*, 11(11):5513–5524, 2015.

[17] O Demerdash, U R Shrestha, L Petridis, J C Smith, J C Mitchell, and A Ramanathan. Using Small-Angle Scattering Data and Parametric Machine Learning to Optimize Force Field Parameters for Intrinsically Disordered Proteins. *Front Mol Biosci*, 6:64, 2019.

[18] J Mu, H Liu, J Zhang, R Luo, and H F Chen. Recent Force Field Strategies for Intrinsically Disordered Proteins. *J Chem Inf Model*, 61(3):1037–1047, 2021.

[19] J Huang, S Rauscher, G Nawrocki, T Ran, M Feig, B L de Groot, H Grubmüller, and A D MacKerell. CHARMM36m: an improved force field for folded and intrinsically disordered proteins. *Nat Methods*, 14(1):71–73, 2017.

[20] P Robustelli, S Piana, and D E Shaw. Developing a molecular dynamics force field for both folded and disordered protein states. *Proc Natl Acad Sci U S A*, 115(21):E4758–E4766, 2018.

[21] S Piana, P Robustelli, D Tan, S Chen, and D E Shaw. Development of a Force Field for the Simulation of Single-Chain Proteins and Protein-Protein Complexes. *J Chem Theory Comput*, 16(4):2494–2507, 2020.

[22] Y Ding, K Yu, and J Huang. Data science techniques in biomolecular force field development. *Curr Opin Struct Biol*, 78:102502, 2023.

[23] L P Wang, J Chen, and T Van Voorhis. Systematic Parametrization of Polarizable Force Fields from Quantum Chemistry Data. *J Chem Theory Comput*, 9(1):452–460, 2013.

[24] T Fröhlking, M Bernetti, N Calonaci, and G Bussi. Toward empirical force fields that match experimental observables. *J Chem Phys*, 152(23):230902, 2020.

[25] P S Nerenberg and T Head-Gordon. New developments in force fields for biomolecular simulations. *Curr Opin Struct Biol*, 49:129–138, 2018.

[26] A Arsiccio, R Pisano, and J E Shea. A New Transfer Free Energy Based Implicit Solvation Model for the Description of Disordered and Folded Proteins. *J Phys Chem B*, 126(33):6180–6190, 2022.

[27] A Vitalis and R V Pappu. ABSINTH: a new continuum solvation model for simulations of polypeptides in aqueous solutions. *J Comput Chem*, 30(5):673–699, 2009.

[28] F E Thomasen, F Pesce, M A Roesgaard, G Tesei, and K Lindorff-Larsen. Improving Martini 3 for Disordered and Multidomain Proteins. *J Chem Theory Comput*, 18(4):2033–2041, 2022.

[29] G Tesei, T K Schulze, R Crehuet, and K Lindorff-Larsen. Accurate model of liquid-liquid phase behavior of intrinsically disordered proteins from optimization of single-chain properties. *Proc Natl Acad Sci U S A*, 118(44): e2111696118, 2021.

[30] B Strodel. Amyloid aggregation simulations: challenges, advances and perspectives. *Curr Opin Struct Biol*, 67: 145–152, 2021.

[31] I M Ilie and A Caflisch. Simulation Studies of Amyloidogenic Polypeptides and Their Aggregates. *Chem Rev*, 119 (12):6956–6993, 2019.

[32] R B Best, W Zheng, and J Mittal. Balanced Protein-Water Interactions Improve Properties of Disordered Proteins and Non-Specific Protein Association. *J Chem Theory Comput*, 10(11):5113–5124, 2014.

[33] S Piana, A G Donchev, P Robustelli, and D E Shaw. Water dispersion interactions strongly influence simulated structural properties of disordered protein states. *J Phys Chem B*, 119(16):5113–5123, 2015.

[34] P S Shabane, S Izadi, and A V Onufriev. General Purpose Water Model Can Improve Atomistic Simulations of Intrinsically Disordered Proteins. *J Chem Theory Comput*, 15(4):2620–2634, 2019.

[35] P S Nerenberg, B Jo, C So, A Tripathy, and T Head-Gordon. Optimizing solute-water van der Waals interactions to reproduce solvation free energies. *J Phys Chem B*, 116(15):4524–4534, 2012.

[36] M K Robinson, J I Monroe, and M S Shell. Are AMBER Force Fields and Implicit Solvation Models Additive? A Folding Study with a Balanced Peptide Test Set. *J Chem Theory Comput*, 12(11):5631–5642, 2016.

[37] A G Baydin, B A Pearlmutter, A A Radul, and J M Siskind. Automatic differentiation in machine learning: a survey. *Journal of Machine Learning Research*, 18(1):1–43, 2018.

[38] C Rackauckas, A Edelman, K Fischer, M Innes, E Saba, V B Shah, and W Tebbutt. Generalized Physics-Informed Learning Through Language-Wide Differentiable Programming. *CEUR Workshop Proceedings*, 2587, 2020.

[39] J G Greener and D T Jones. Differentiable molecular simulation can learn all the parameters in a coarse-grained force field for proteins. *PLoS One*, 16(9):e0256990, 2021.

[40] W Wang, Z Wu, J C B Dietschreit, and R Gómez-Bombarelli. Learning pair potentials using differentiable simulations. *J Chem Phys*, 158(4):044113, 2023.

[41] W Wang, S Axelrod, and R Gómez-Bombarelli. Differentiable Molecular Simulations for Control and Learning. *arXiv*, 2003.00868, 2020.

[42] M Šípka, J C B Dietschreit, L Grajciar, and R Gómez-Bombarelli. Differentiable Simulations for Enhanced Sampling of Rare Events. *Proceedings of the 40th International Conference on Machine Learning*, 202, 2023.

[43] J Ingraham, A Riesselman, C Sander, and D Marks. Learning Protein Structure with a Differentiable Simulator. *ICLR*, 2019.

[44] C P Goodrich, E M King, S S Schoenholz, E D Cubuk, and M P Brenner. Designing self-assembling kinetics with differentiable statistical physics models. *Proc Natl Acad Sci U S A*, 118(10):e2024083118, 2021.

[45] S S Schoenholz and E D Cubuk. JAX, M.D. A Framework for Differentiable Physics. *Advances in Neural Information Processing Systems*, 33, 2020.

[46] S Doerr, M Majewski, A Pérez, A Krämer, C Clementi, F Noe, T Giorgino, and G De Fabritiis. TorchMD: A Deep Learning Framework for Molecular Simulations. *J Chem Theory Comput*, 17(4):2355–2363, 2021.

[47] X Wang, J Li, L Yang, F Chen, Y Wang, J Chang, J Chen, L Zhang, and K Yu. DMFF: An Open-Source Automatic Differentiable Platform for Molecular Force Field Development and Molecular Dynamics Simulation. *ChemRxiv*, `https://chemrxiv.org/engage/chemrxiv/article-details/637d7f440146efb7290215ca`, 2022.

[48] Jeff Bezanson, Alan Edelman, Stefan Karpinski, and Viral B Shah. Julia: A fresh approach to numerical computing. *SIAM Review*, 59(1):65–98, 2017.

[49] E Roesch, J G Greener, A L MacLean, H Nassar, C Rackauckas, T E Holy, and M P H Stumpf. Julia for biologists. *Nat Methods*, 20(5):655–664, 2023.

[50] Tim Besard, Christophe Foket, and Bjorn De Sutter. Effective Extensible Programming: Unleashing Julia on GPUs. *IEEE Transactions on Parallel and Distributed Systems*, 30(4):827–841, 2019.

[51] Tim Besard, Valentin Churavy, Alan Edelman, and Bjorn De Sutter. Rapid software prototyping for heterogeneous and distributed platforms. *Advances in Engineering Software*, 132:29–46, 2019.

[52] M Innes. Don't Unroll Adjoint: Differentiating SSA-Form Programs. *arXiv*, 1810.07951, 2018.

[53] W Moses and V Churavy. Instead of Rewriting Foreign Code for Machine Learning, Automatically Synthesize Fast Gradients. *Advances in Neural Information Processing Systems*, 33:12472–12485, 2020.

[54] W S Moses, V Churavy, L Paehler, J Hückelheim, S H K Narayanan, M Schanen, and J Doerfert. Reverse-Mode Automatic Differentiation and Optimization of GPU Kernels via Enzyme. *Proceedings of the International Conference for High Performance Computing, Networking, Storage and Analysis*, 2021.

[55] J Revels, T Besard, V Churavy, B De Sutter, and J P Vielma. Dynamic Automatic Differentiation of GPU Broadcast Kernels. *arXiv*, 1810.08297, 2018.

[56] H Nguyen, D R Roe, and C Simmerling. Improved Generalized Born Solvent Model Parameters for Protein Simulations. *J Chem Theory Comput*, 9(4):2020–2034, 2013.

[57] S Bottaro, K Lindorff-Larsen, and R B Best. Variational Optimization of an All-Atom Implicit Solvent Force Field to Match Explicit Solvent Simulation Data. *J Chem Theory Comput*, 9(12):5641–5652, 2013.

[58] W Kang, F Jiang, and Y D Wu. How to strike a conformational balance in protein force fields for molecular dynamics simulations? *WIREs Comput Mol Sci*, 12(3):e1578, 2022.

[59] J E Kohn, I S Millett, J Jacob, B Zagrovic, T M Dillon, N Cingel, R S Dothager, S Seifert, P Thiyagarajan, T R Sosnick, M Z Hasan, V S Pande, I Ruczinski, S Doniach, and K W Plaxco. Random-coil behavior and the dimensions of chemically unfolded proteins. *Proc Natl Acad Sci U S A*, 101(34):12491–12496, 2004.

[60] J A Maier, C Martinez, K Kasavajhala, L Wickstrom, K E Hauser, and C Simmerling. ff14SB: Improving the Accuracy of Protein Side Chain and Backbone Parameters from ff99SB. *J Chem Theory Comput*, 11(8):3696–3713, 2015.

[61] P Robustelli, A Ibanez-de Opakua, C Campbell-Bezat, F Giordanetto, S Becker, M Zweckstetter, A C Pan, and D E Shaw. Molecular Basis of Small-Molecule Binding to α-Synuclein. *J Am Chem Soc*, 144(6):2501–2510, 2022.

[62] L Tatenhorst, K Eckermann, V Dambeck, L Fonseca-Ornelas, H Walle, T Lopes da Fonseca, J C Koch, S Becker, L Tönges, M Bähr, T F Outeiro, M Zweckstetter, and P Lingor. Fasudil attenuates aggregation of α-synuclein in models of Parkinson's disease. *Acta Neuropathol Commun*, 4:39, 2016.

[63] P H Nguyen, M S Li, and P Derreumaux. Effects of all-atom force fields on amyloid oligomerization: replica exchange molecular dynamics simulations of the $A\beta_{16\text{-}22}$ dimer and trimer. *Phys Chem Chem Phys*, 13(20):9778–9788, 2011.

[64] S Samantray, F Yin, B Kav, and B Strodel. Different Force Fields Give Rise to Different Amyloid Aggregation Pathways in Molecular Dynamics Simulations. *J Chem Inf Model*, 60(12):6462–6475, 2020.

[65] D van der Spoel. Systematic design of biomolecular force fields. *Curr Opin Struct Biol*, 67:18–24, 2021.

[66] X Fu, Z Wu, W Wang, T Xie, S Keten, R Gómez-Bombarelli, and T S Jaakkola. Forces are not Enough: Benchmark and Critical Evaluation for Machine Learning Force Fields with Molecular Simulations. *TMLR*, 2023.

[67] J Hückelheim, H Menon, W Moses, B Christianson, P Hovland, and L Hascoët. Understanding Automatic Differentiation Pitfalls. *arXiv*, 2305.07546, 2023.

[68] Y Wang, J Fass, B Kaminow, J E Herr, D Rufa, I Zhang, I Pulido, M Henry, H E Bruce Macdonald, K Takaba, and J D Chodera. End-to-end differentiable construction of molecular mechanics force fields. *Chem Sci*, 13(41): 12016–12033, 2022.

[69] J T Horton, S Boothroyd, P K Behara, D L Mobley, and D J Cole. A transferable double exponential potential for condensed phase simulations of small molecules. *Digital Discovery*, 2023.

[70] L Metz, C D Freeman, S S Schoenholz, and T Kachman. Gradients are Not All You Need. *arXiv*, 2111.05803, 2021.

[71] Yuanming Hu, Luke Anderson, Tzu-Mao Li, Qi Sun, Nathan Carr, Jonathan Ragan-Kelley, and Frédo Durand. DiffTaichi: Differentiable Programming for Physical Simulation. *ICLR*, 2020.

[72] H J Suh, M Simchowitz, K Zhang, and R Tedrake. Do Differentiable Simulators Give Better Policy Gradients? *Proceedings of the 39th International Conference on Machine Learning*, 162:20668–20696, 2022.

[73] P Kidger. On Neural Differential Equations. *arXiv*, 2202.02435, 2022.

[74] Y Ma, V Dixit, M J Innes, X Guo, and C Rackauckas. A Comparison of Automatic Differentiation and Continuous Sensitivity Analysis for Derivatives of Differential Equation Solutions. *HPEC*, 2021.

[75] P Eastman, J Swails, J D Chodera, R T McGibbon, Y Zhao, K A Beauchamp, L P Wang, A C Simmonett, M P Harrigan, C D Stern, R P Wiewiora, B R Brooks, and V S Pande. OpenMM 7: Rapid development of high performance algorithms for molecular dynamics. *PLoS Comput Biol*, 13(7):e1005659, 2017.

[76] M J Abraham, T Murtola, R Schulz, S Páll, J C Smith, B Hess, and E Lindahl. GROMACS: High performance molecular simulations through multi-level parallelism from laptops to supercomputers. *SoftwareX*, 1-2:19–25, 2015.

[77] J Srinivasan, M W Trevathan, P Beroza, and D A Case. Application of a pairwise generalized Born model to proteins and nucleic acids: inclusion of salt effects. *Theor Chem Acc*, 101:426–434, 1999.

[78] R J Gowers, M Linke, J Barnoud, T J E Reddy, M N Melo, S L Seyler, J Domański, D L Dotson, S Buchoux, I M Kenney, and O Beckstein. MDAnalysis: A Python Package for the Rapid Analysis of Molecular Dynamics Simulations. *Proceedings of the 15th Python in Science Conference*, pages 98–105, 2016.

[79] R T McGibbon, K A Beauchamp, M P Harrigan, C Klein, J M Swails, C X Hernández, C R Schwantes, L-P Wang, T J Lane, and V S Pande. MDTraj: A Modern Open Library for the Analysis of Molecular Dynamics Trajectories. *Biophysical Journal*, 109(8):1528–1532, 2015.

[80] J G Greener, J Selvaraj, and B J Ward. BioStructures.jl: read, write and manipulate macromolecular structures in Julia. *Bioinformatics*, 36(14):4206–4207, 2020.

[81] J Wang, R M Wolf, J W Caldwell, P A Kollman, and D A Case. Development and testing of a general amber force field. *J Comput Chem*, 25(9):1157–1174, 2004.

[82] L Martínez, R Andrade, E G Birgin, and J M Martínez. PACKMOL: a package for building initial configurations for molecular dynamics simulations. *J Comput Chem*, 30(13):2157–2164, 2009.

Supplementary Data

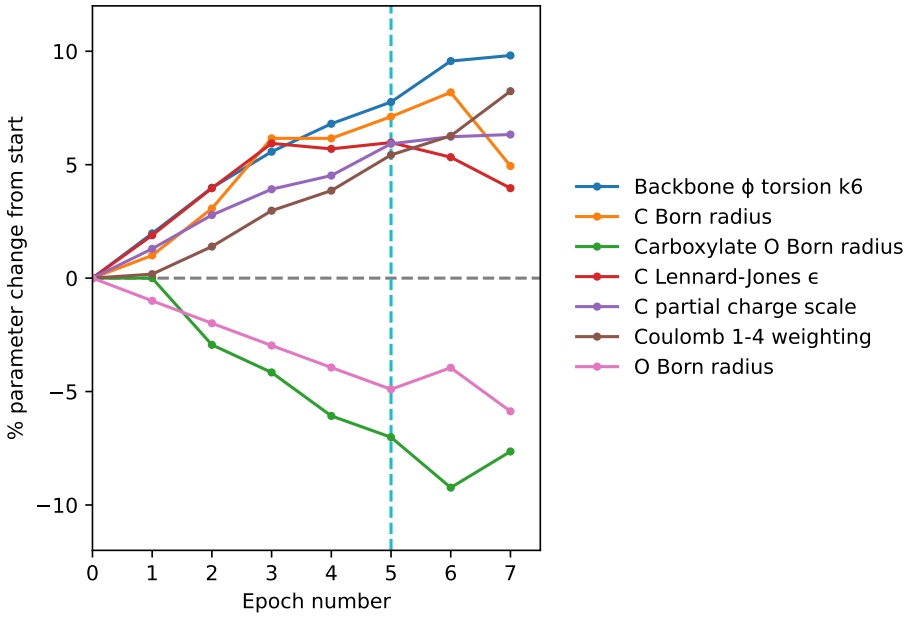

Figure S1 Parameter changes during training. The 7 parameters that change by at least 4.5% in absolute value from the starting values in a99SB-*disp*+GBNeck2 are shown. Parameters after epoch 5 were used in GB99dms, as indicated by a cyan line.

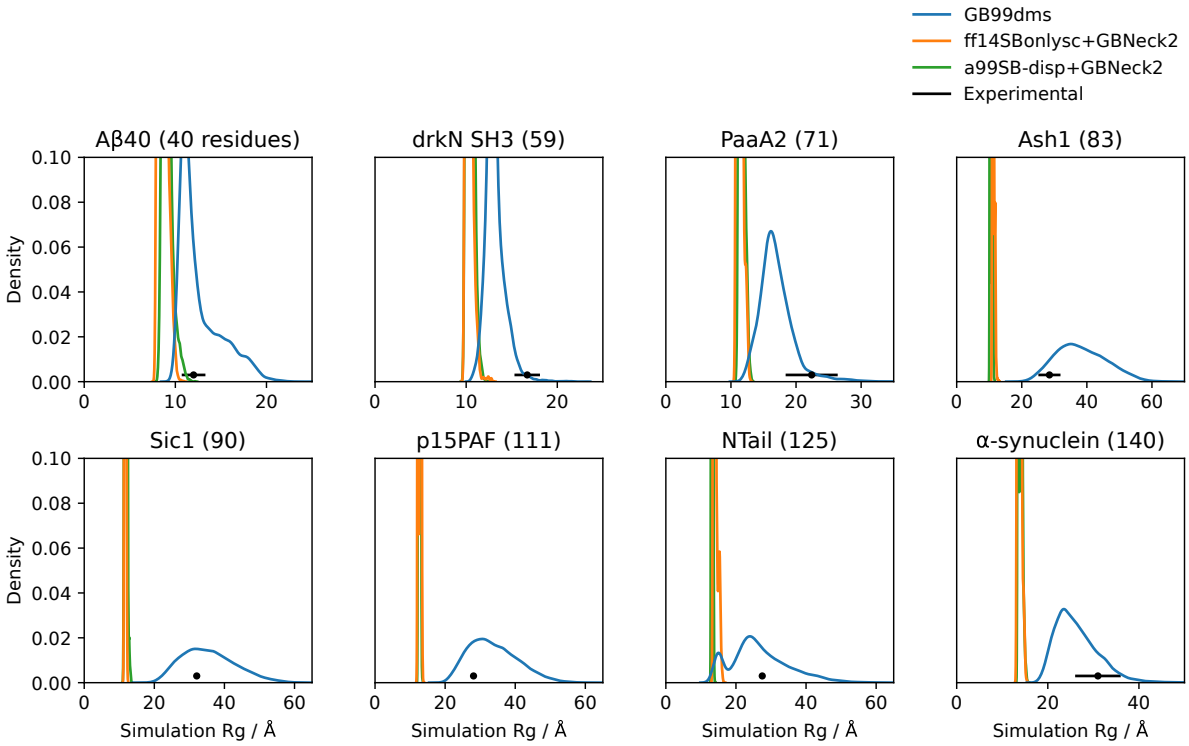

Figure S2 Radius of gyration of IDPs with implicit solvent force fields. Each distribution is the R_g over 3 simulations of 2 µs, with an initial burn-in period of 0.5 µs starting from an extended conformation being discarded for each simulation. Experimental values are taken from Robustelli et al. 2018 [20] and the error bars represent uncertainty in the experimental value.

Table S1 Parameters in GB99dms. The other parameters not changed during training are the same as in a99SB-*disp* or GBNeck2. The atom type HO LJ parameters are zero in a99SB-*disp* so are not modified. This table is available in CSV format in the data repository.

Parameter	**Value in GB99dms**	**Value in a99SB-*disp* or GBNeck2**	**Change over training**	**% change over training**
atom CA charge scale	0.996	1.0	-0.00395	-0.39%
atom CA LJ σ / nm	0.342	0.34	0.00183	0.54%
atom CA LJ ε / kJ mol^{-1}	0.364	0.36	0.00452	1.26%
atom CT charge scale	1.01	1.0	0.0104	1.04%
atom CT LJ σ / nm	0.337	0.34	-0.00304	-0.89%
atom CT LJ ε / kJ mol^{-1}	0.447	0.458	-0.0111	-2.43%
atom C charge scale	1.06	1.0	0.0592	5.92%
atom C LJ σ / nm	0.352	0.34	0.0117	3.43%
atom C LJ ε / kJ mol^{-1}	0.381	0.36	0.0215	5.98%
atom C8 charge scale	0.999	1.0	-0.000894	-0.09%
atom C8 LJ σ / nm	0.339	0.34	-0.000537	-0.16%
atom C8 LJ ε / kJ mol^{-1}	0.457	0.458	-0.00115	-0.25%
atom C9 charge scale	1.0	1.0	-7.96e-05	-0.01%
atom C9 LJ σ / nm	0.339	0.34	-0.000495	-0.15%
atom C9 LJ ε / kJ mol^{-1}	0.456	0.458	-0.00204	-0.45%
atom N charge scale	1.0	1.0	0.00188	0.19%
atom N LJ σ / nm	0.339	0.325	0.0135	4.16%
atom N LJ ε / kJ mol^{-1}	0.737	0.711	0.026	3.66%
atom N3 charge scale	0.999	1.0	-0.000968	-0.10%
atom N3 LJ σ / nm	0.325	0.325	0.000179	0.05%
atom N3 LJ ε / kJ mol^{-1}	0.711	0.711	0.000102	0.01%
atom O charge scale	1.01	1.0	0.00632	0.63%
atom O LJ σ / nm	0.296	0.296	0.000153	0.05%
atom O LJ ε / kJ mol^{-1}	0.863	0.879	-0.0159	-1.81%
atom O2 charge scale	1.01	1.0	0.00893	0.89%
atom O2 LJ σ / nm	0.298	0.296	0.00192	0.65%
atom O2 LJ ε / kJ mol^{-1}	0.879	0.879	0.000523	0.06%
atom OH charge scale	1.0	1.0	0.00111	0.11%
atom OH LJ σ / nm	0.305	0.307	-0.00125	-0.41%
atom OH LJ ε / kJ mol^{-1}	0.879	0.88	-0.00152	-0.17%
atom H charge scale	1.0	1.0	0.000143	0.01%
atom H LJ σ / nm	0.105	0.107	-0.00178	-1.66%
atom H LJ ε / kJ mol^{-1}	0.065	0.0657	-0.000736	-1.12%
atom H1 charge scale	1.0	1.0	-9.15e-05	-0.01%
atom H1 LJ σ / nm	0.246	0.247	-0.00136	-0.55%
atom H1 LJ ε / kJ mol^{-1}	0.0656	0.0657	-0.000109	-0.17%
atom HA charge scale	1.0	1.0	-9.91e-06	-0.00%
atom HA LJ σ / nm	0.261	0.26	0.000723	0.28%
atom HA LJ ε / kJ mol^{-1}	0.063	0.0628	0.00022	0.35%
atom HC charge scale	1.0	1.0	-0.000251	-0.03%
atom HC LJ σ / nm	0.259	0.265	-0.00634	-2.39%
atom HC LJ ε / kJ mol^{-1}	0.0637	0.0657	-0.00201	-3.06%
atom HO charge scale	1.0	1.0	-9.49e-05	-0.01%
atom HP charge scale	1.0	1.0	2.04e-05	0.00%
atom HP LJ σ / nm	0.196	0.196	0.000429	0.22%
atom HP LJ ε / kJ mol^{-1}	0.0658	0.0657	8.14e-05	0.12%

Parameter	**Value in GB99dms**	**Value in a99SB-*disp* or GBNeck2**	**Change over training**	**% change over training**
Lennard-Jones 1-4 weighting	0.51	0.5	0.00979	1.96%
Coulomb 1-4 weighting	0.879	0.833	0.0452	5.43%
torsion -/C/N/- k1 / kJ mol^{-1}	-10.5	-10.5	0.00207	0.02%
torsion -/CA/CA/- k1 / kJ mol^{-1}	-15.2	-15.2	-7.93e-06	-0.00%
torsion -/CT/C8/- k1 / kJ mol^{-1}	0.648	0.649	-0.00068	-0.10%
torsion -/CT/C9/- k1 / kJ mol^{-1}	0.649	0.649	0.000208	0.03%
torsion -/CT/CT/- k1 / kJ mol^{-1}	0.655	0.651	0.00405	0.62%
torsion -/CT/N3/- k1 / kJ mol^{-1}	0.651	0.651	6.06e-05	0.01%
torsion C/N/CT/C k1 / kJ mol^{-1}	-0.14	-0.142	0.00256	1.80%
torsion C/N/CT/C k2 / kJ mol^{-1}	1.4	1.4	0.000432	0.03%
torsion C/N/CT/C k3 / kJ mol^{-1}	2.27	2.28	-0.00382	-0.17%
torsion C/N/CT/C k4 / kJ mol^{-1}	0.332	0.335	-0.00223	-0.67%
torsion C/N/CT/C k5 / kJ mol^{-1}	1.67	1.67	-0.00378	-0.23%
torsion CT/CT/C/N k1 / kJ mol^{-1}	0.837	0.837	-0.000137	-0.02%
torsion CT/CT/C/N k2 / kJ mol^{-1}	0.837	0.837	0.000467	0.06%
torsion CT/CT/C/N k3 / kJ mol^{-1}	1.67	1.67	-0.00251	-0.15%
torsion CT/CT/N/C k1 / kJ mol^{-1}	8.37	8.37	-0.00109	-0.01%
torsion CT/CT/N/C k2 / kJ mol^{-1}	8.37	8.37	0.00268	0.03%
torsion CT/CT/N/C k3 / kJ mol^{-1}	1.67	1.67	-0.0032	-0.19%
torsion H/N/C/O k1 / kJ mol^{-1}	8.37	8.37	1.84e-05	0.00%
torsion H/N/C/O k2 / kJ mol^{-1}	-10.5	-10.5	-7.33e-05	-0.00%
torsion H1/CT/C/O k1 / kJ mol^{-1}	3.35	3.35	0.000823	0.02%
torsion H1/CT/C/O k2 / kJ mol^{-1}	-0.332	-0.335	0.00321	0.96%
torsion HC/CT/C4/CT k1 / kJ mol^{-1}	0.67	0.669	0.000134	0.02%
torsion N/CT/C/N k1 / kJ mol^{-1}	2.72	2.72	-0.00113	-0.04%
torsion N/CT/C/N k2 / kJ mol^{-1}	-0.825	-0.824	-0.000732	-0.09%
torsion N/CT/C/N k3 / kJ mol^{-1}	6.05	6.05	0.000215	0.00%
torsion N/CT/C/N k4 / kJ mol^{-1}	2.0	2.0	0.000106	0.01%
torsion N/CT/C/N k5 / kJ mol^{-1}	-0.0776	-0.0799	0.00232	2.90%
torsion N/CT/C/N k6 / kJ mol^{-1}	-0.0154	-0.0167	0.0013	7.76%
torsion N/CT/C/N k7 / kJ mol^{-1}	-1.07	-1.07	0.0	0.00%
torsion N/CT/C/N k8 / kJ mol^{-1}	0.314	0.314	0.0	0.00%
torsion N/CT/C/N k9 / kJ mol^{-1}	0.238	0.238	0.0	0.00%
torsion N/CT/C/N k10 / kJ mol^{-1}	0.105	0.105	0.0	0.00%
torsion N/CT/C/N k11 / kJ mol^{-1}	-0.046	-0.046	0.0	0.00%

Parameter	**Value in GB99dms**	**Value in a99SB-*disp* or GBNeck2**	**Change over training**	**% change over training**
GB atom radius C / nm	0.182	0.17	0.0121	7.12%
GB atom radius N / nm	0.153	0.155	-0.002	-1.29%
GB atom radius O / nm	0.143	0.15	-0.00735	-4.90%
GB atom radius O_CAR / nm	0.13	0.14	-0.00982	-7.01%
GB atom radius H / nm	0.124	0.12	0.00431	3.59%
GB atom radius H_N / nm	0.125	0.13	-0.00504	-3.88%
GB atom parameter α C	0.75	0.734	0.016	2.18%
GB atom parameter β C	0.487	0.506	-0.0197	-3.89%
GB atom parameter γ C	0.214	0.206	0.00859	4.17%
GB atom parameter α N	0.507	0.503	0.00391	0.78%
GB atom parameter β N	0.318	0.317	0.0013	0.41%
GB atom parameter γ N	0.191	0.193	-0.00227	-1.18%
GB atom parameter α O	0.837	0.868	-0.0313	-3.60%
GB atom parameter β O	0.899	0.877	0.0227	2.59%
GB atom parameter γ O	0.389	0.388	0.00134	0.35%
GB atom parameter α H	0.788	0.788	-0.000574	-0.07%
GB atom parameter β H	0.799	0.799	0.000786	0.10%
GB atom parameter γ H	0.436	0.437	-0.00122	-0.28%
GB screening parameter C	1.1	1.06	0.0456	4.30%
GB screening parameter N	0.736	0.734	0.00278	0.38%
GB screening parameter O	1.07	1.06	0.00517	0.49%
GB screening parameter H	1.43	1.43	0.000751	0.05%
GB neck cutoff / nm	0.68	0.68	0.0	0.00%
GB neck scale	0.853	0.827	0.0257	3.11%
GB offset / nm	0.0195	0.0195	-1.38e-05	-0.07%
GB probe radius / nm	0.134	0.14	-0.00574	-4.10%
GB SA factor / kJ mol^{-1} nm^{-2}	28.4	28.4	-0.000219	-0.00%